





Oxygen vacancies in KTiOPO_4 : Optical absorption from hybrid DFT

A. Bocchini ^{*}, U. Gerstmann , and W. G. Schmidt 

Lehrstuhl für Theoretische Materialphysik, Universität Paderborn, Paderborn 33098, Germany

 (Received 8 November 2021; revised 25 April 2022; accepted 26 April 2022; published 16 May 2022)

Density functional theory is used to calculate the optical absorption of oxygen vacancies in potassium titanyl phosphate (KTiOPO_4 , KTP) crystals. A modified hybrid functional is used for the description of the midgap defect states and the optical excitation energies. Oxygen vacancies in the +2 charge state lead to rather minor modification of the bulk KTP optical response, while the +1 and neutral charge states give rise to characteristic midgap optical absorption covering the whole near-infrared and visible spectrum. Its intensity is strongly polarization dependent and strongest for light polarized parallel to the z axis. The modification of the KTP optical absorption by oxygen vacancies predicted here corroborates the picture that the gray-track formation in KTP, i.e., its photochromic damage, is related to a successive charging of oxygen vacancies.

DOI: [10.1103/PhysRevB.105.205118](https://doi.org/10.1103/PhysRevB.105.205118)

I. INTRODUCTION

Ferroelectric potassium titanyl phosphate (KTiOPO_4 , KTP) is an excellent material for nonlinear-optical devices. Its broad transparency band (350–4500 nm) [1] and large nonlinear-optical coefficients together with high damage thresholds [1–4] make it suitable, e.g., for frequency doubling in Nd:YAG lasers [5]. Its application, however, is limited by a phenomenon called gray tracking: The gray tracks form when KTP crystals are, e.g., exposed to strong electric fields [6] or irradiated with high-intensity laser light [7,8]. Dark channels, i.e., regions with strongly reduced transmission, appear along the propagation of [001] polarized laser beams [9]. In addition to decreasing the optical transmission [8,9], the gray tracks increase the optical anisotropy [7]. The transmission can be restored, and the dark traces are quenched upon annealing in wet oxygen [10] or at 200 °C [11]. Gray tracks absorb both the fundamental and the second-harmonic radiation, and the continued operation after their appearance can lead to device failure [6,10,12].

KTP forms an orthorhombic crystal with a 64-atom unit cell, space group $Pna2_1$, and lattice parameters $a = 12.814$ Å, $b = 6.404$ Å, and $c = 10.616$ Å [1,13,14]; see Fig. 1. The Ti, P, and O atoms form TiO_6 octahedra and PO_4 tetrahedra linked via mutual oxygens to chains along the [100] and [010] directions. Thus the O sites can be classified according to their coordination: O(1)–O(8) are coordinated with P and Ti, while O(9) and O(10) are located between two Ti atoms [1,13,14,16]. The K atoms form a positively charged sublattice with K(1) and K(2) coordinated with eight and nine O atoms, respectively [13]. The $\text{KO}_{8,9}$ units [17] together with the distorted TiO_6 octahedra [2] are believed to cause the strong optical nonlinearity of the material. The K atoms are only weakly bonded and show high mobilities along [001] [13]. As a consequence, KTP crystals may be affected by

high K-vacancy concentrations that are charge compensated by other defects [13]. Notably, crystals with a high K-vacancy concentration are found to be particularly affected by gray tracking [13,18].

The mechanisms leading to gray tracking are still a matter of research and far from being completely understood. K vacancies do not provide any midgap states and thus cannot contribute directly to the observed absorption [19]. The emergence of gray tracks is frequently discussed to be related to the reduction of Ti atoms (from 4+ to 3+) resulting from charge compensation, i.e., electron capture from O vacancies or other intrinsic or extrinsic defect centers [6,11,12,20–23]. In fact, several Ti^{3+} defect centers have been detected in gray-track-affected samples by electron paramagnetic resonance (EPR) [6,20,21] and electron nuclear double resonance (ENDOR) spectroscopy [20,21]. However, only one of them is stable at room temperature [21]. It has been unambiguously attributed to the positively charged O vacancy $V_{\text{O}(10)}^{+1}$ [21,24]. In addition to the EPR-active +1 charge state, its +2 and neutral charge states are also thermodynamically stable [24] and may be thus relevant for gray tracking.

This motivates the present work, which extends earlier studies by some of the present authors on the KTP optical response [25] and point defects characteristic to KTP [19,24]. Here, we use hybrid density functional theory to calculate the optical absorption of KTP hosting V_{O} vacancies. In the case of $V_{\text{O}(10)}$, the occurrence of characteristic midgap absorption is found. It is strongly dependent on the defect charge state as well as the polarization of the incident light and thus suitable to explain the experimental observations in the early stage of gray tracking. This suggests that $V_{\text{O}(10)}$ vacancies not only play an important role in charge compensation, but also are directly involved in the photochromic damage.

II. METHODOLOGY

The determination of the ground-state geometries in this paper is based on density functional theory (DFT) as

^{*}adrianab@mail.upb.de

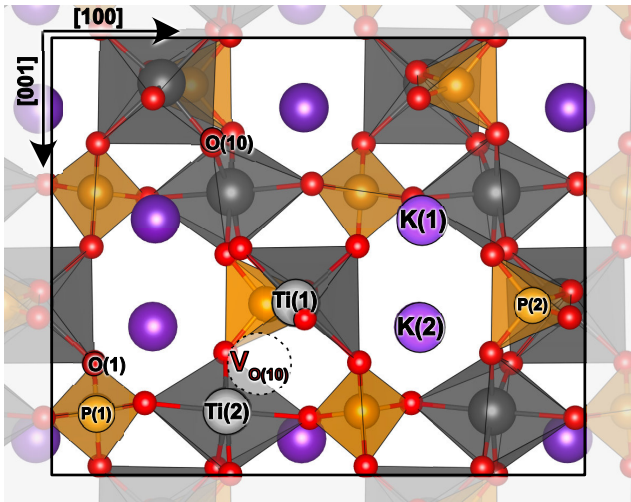


FIG. 1. Schematic representation [15] of the KTP unit cell. Red, orange, gray, and purple atoms correspond to O, P, Ti, and K atoms, respectively. The position of the vacancy $V_{O(10)}$ before geometry relaxation is indicated, too.

implemented in the open-source package QUANTUM ESPRESSO (QE) [26,27]. The calculations are performed for 64-atom supercells using periodic boundary conditions. The electron-ion interactions are modeled via norm-conserving pseudopotentials that treat the Ti $3d^3 4s^1$, P $3s^2 3p^3$, K $4s^1$, and O $2s^2 2p^4$ states as valence states. The electron exchange and correlation (XC) effects are described within the generalized gradient approximation (GGA) using the revised Perdew-Burke-Ernzerhof functional PBEsol [28]. Additionally, a 5.1-eV Hubbard [24,29] energy correction is applied to the Ti $3d$ states. In principle, changes in the local chemical environment within the oxide can be taken into account by using site-dependent U values [29–31]. However, in Ref. [24] we have determined the Hubbard- U values for O vacancies in KTP self-consistently and found values that do not deviate by more than ± 0.25 eV from 5.1 eV. Hence, for the sake of simplicity, we use this average value throughout this paper. Thereby, we use the simplified version given by Cococcioni and de Gironcoli [29], using an effective Hubbard- U value and atomic wave functions to build the required projectors on localized orbitals. This PBEsol + U methodology allows for the highly accurate modeling of KTP bulk and defect structures as verified earlier by comparison of calculated and measured magnetic signatures of KTP defects [24]. Optical response calculations are performed within the independent-particle approximation (IPA) using the open-source code YAMBO [32,33] based on the geometries structurally optimized within PBEsol + U . The Brillouin zone is sampled with a $3 \times 6 \times 3$ Γ -centered mesh, which ensures well-converged optical spectra.

DFT with (semi)local exchange-correlation (XC) functionals typically suffers from an underestimation of the single-particle excitation energies. Therefore optical absorption spectra calculated within the IPA based on the DFT electron structure typically agree with experiment only qualitatively [34]. The calculated excitation energies are redshifted compared with the measured data. A more

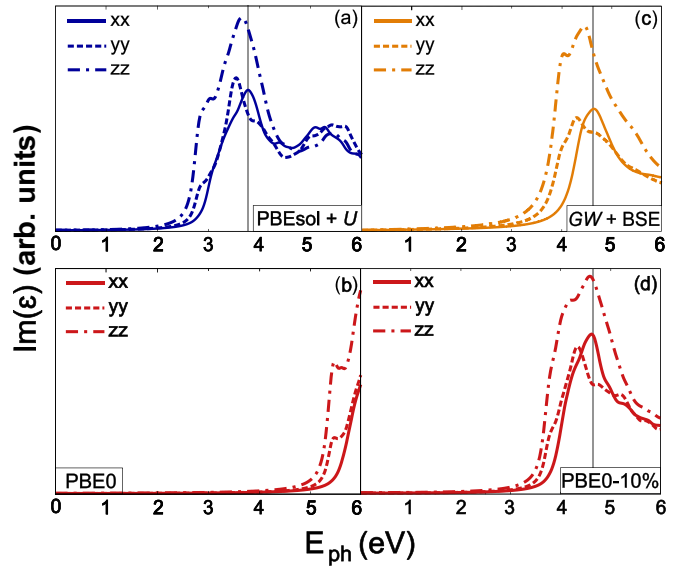


FIG. 2. The imaginary part (diagonal components referring to the crystal axes) of the dielectric function ϵ of a KTP unit cell calculated using (a) a Hubbard correction of $U = 5.1$ eV on the Ti $3d$ states, (b) the hybrid PBE0 with the standard fraction $\alpha = 25\%$ of EXX, (c) the $GW + BSE$ approach [25], and (d) a modification of PBE0 with $\alpha = 10\%$ (PBE0-10%) of EXX. E_{ph} , photon energy.

realistic description of the experiment is obtained using the independent-quasiparticle approximation (IQA), which accounts for electronic self-energy effects [34]. Realistic quasiparticle energies may be obtained by calculating self-energy corrections within the GW approximation [35,36] (DFT + GW). The subsequent solution of the Bethe-Salpeter equation (BSE) allows one to account for excitonic effects and leads to a redistribution of oscillator strengths to lower excitation energies, often partially compensating the blueshift resulting from the self-energy corrections [36–39]. The combined $GW + BSE$ methodology typically results in calculated optical spectra in close agreement with experiment. This holds also for KTP [see Fig. 2(c)], where a self-energy blueshift of about 2 eV is partially compensated by an excitonic redshift of about 1.5 eV; see discussion in Ref. [25]. For comparison, the $GW + BSE$ approach has been applied in this paper to one defect structure, the $V_{O(1)}$ vacancy. These calculations are numerically on the same footing as used in Ref. [25]. The large unit cell in conjunction with the low symmetry forced us, however, to reduce the k -point sampling to the Γ -centered $1 \times 2 \times 1$ mesh.

The success of the GW approximation, at least in the case of non-self-consistent GW , depends on the quality of the electronic structure on which it is based. This renders its application to $V_{O(10)}$ difficult: The use of (semi)local functionals such as PBEsol leads to delocalized defect states within the KTP conduction band [see Fig. 3(a)]. Consequently, DFT-PBEsol places the charge transition levels (+2/+1) and (+1/0) above the band gap and fails to describe the EPR-active $V_{O(10)}^{+1}$ state. Its modeling requires a Hubbard energy correction $U = 5.1$ eV on the Ti $3d$ states [24]. Unfortunately, this PBEsol + U approach, while providing an occupied midgap defect state [see Fig. 3(b)], still suffers from an

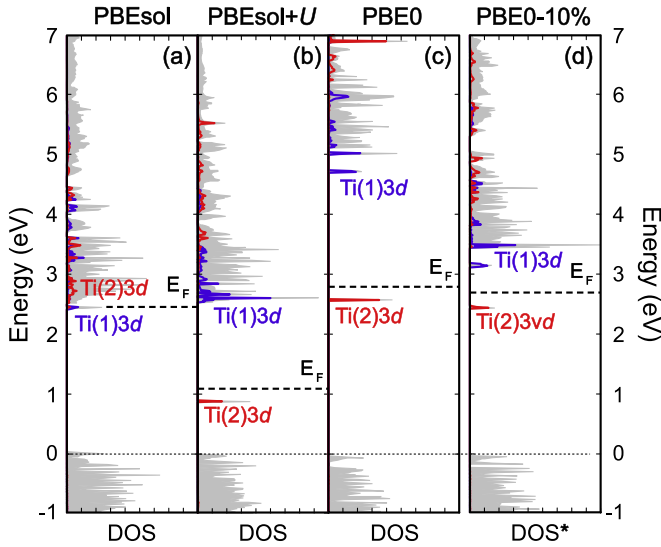


FIG. 3. Electronic density of states (DOS) of $V_{O(10)}^{+1}$ calculated on different levels of theory. Self-consistently determined geometries were used for the PBEsol and PBEsol + U calculations. The latter geometry was also employed for the PBE0 and PBE0-10% calculations. The renormalized density of states obtained by using the PBE0-10% scheme is denoted DOS*. The Ti(1) 3d and Ti(2) 3d states highlighted in the figure are located at the Ti atoms near the vacancy (see Fig. 7).

underestimated bulk band gap ($E_g^{\text{expt}} = 3.2\text{--}3.8$ eV [4,40–42] vs $E_g^{\text{PBEsol+}U} = 2.8$ eV) and is not a suitable starting point for optical response calculations [see Fig. 2(a)]. The PBEsol + U calculations could probably provide a valid starting point for self-consistent GW , which is, however, beyond our present computational possibilities, given the size and low symmetry of the defect supercell.

Hybrid DFT is often a viable alternative: An adjustable fraction α of exact exchange (EXX) [43] from Hartree-Fock theory via hybrid functionals is frequently used to correct single-particle excitation energies [44–49]. At the same time, hybrid DFT leads to a more accurate description of strongly localized electronic states and the related defect levels than can be achieved with (semi)local XC functionals [49–51]. The application of the PBE0 functional [52], which describes the electron correlation within the PBE [53] but replaces a fraction $\alpha = 25\%$ of the PBE exchange with Hartree-Fock exchange, leads to a band gap of 5.33 eV for bulk KTP, close to the value of 5.23 eV obtained within the GW approximation [25]. Moreover, we verified that the PBE0 functional leads to defect geometries and hyperfine tensors in close agreement with our previous PBEsol + U results [24]. This provides additional credibility to this approach.

As expected from the large band gap, the dielectric function calculated in the independent-particle approximation (IPA) from the PBE0 electronic structure [Fig. 2(b)] is blueshifted by about 1.5 eV compared with experiment and GW + BSE theory [Fig. 2(c)]. As mentioned above, electronic self-energy effects and electron-hole interaction effects cancel each other to some extent [37–39,54,55]. We exploit this cancellation here by modifying the PBE0. Specifically, we use a reduced EXX fraction $\alpha = 10\%$. This method, called

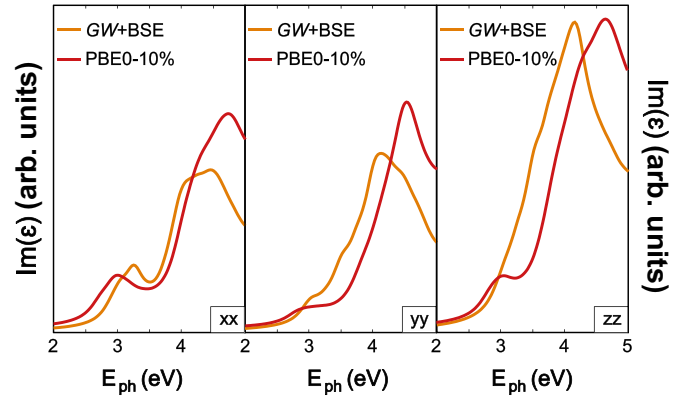


FIG. 4. The imaginary part (diagonal components referring to the crystal axes) of the dielectric function ϵ of a KTP unit cell featuring the vacancy $V_{O(1)}^0$ calculated using the GW + BSE (orange) and the PBE0-10% (red) approach. E_{ph} , photon energy.

PBE0-10% in the following, leads to an IPA bulk optical response in close agreement with the GW + BSE data from Ref. [25]; see Figs. 2(c) and 2(d). The present PBE0-10% calculations are also in qualitative agreement with the BSE data of Ghoohestani *et al.* [56], with respect to both the onset of the optical absorption and the line shapes of the diagonal components of the dielectric function.

The PBE0-10% approach gives rise to an occupied $V_{O(10)}^{+1}$ defect state within the KTP band gap [see Fig. 3(d)]. Similarly to the PBE0 scheme, it is positioned at about 2.4 eV above the valence band maximum. The unoccupied defect states, as well as the KTP conduction band, are lowered by 1.5 eV in PBE0-10% compared with PBE0. This explains the good agreement between the bulk KTP optical spectra based on the PBE0-10% electronic structure with GW + BSE theory. Below we address the question of which accuracy can be expected from PBE0-10% calculations in the case of defect optical signatures.

III. RESULTS AND DISCUSSION

A. Vacancy $V_{O(1)}$

The $V_{O(1)}$ vacancy is located between Ti and P. It is characterized by a strongly localized and twofold occupied defect level. This level is positioned within the KTP band gap already on the DFT-PBEsol level of theory [19]. Therefore it is directly accessible to both GW + BSE and PBE0-10%. It can thus be used to establish error bars relevant for the application of PBE0-10% to defect states.

Figure 4 compares the $V_{O(1)}$ optical absorption spectra calculated on the GW + BSE and PBE0-10% levels of theory. Since there are no additional absorption peaks in the low-energy region, we focus on the energy range 2–5 eV. The spectra agree qualitatively. There are, however, clear differences in the peak positions. On the one hand, the main optical absorption peak characteristic for the bulk is blueshifted within PBE0-10% by up to 0.5 eV. The shift is most pronounced for the zz component. On the other hand, the calculated defect signature is redshifted within PBE0-10% by up to 0.2 eV. Thus we estimate the error bars of our PBE0-10%

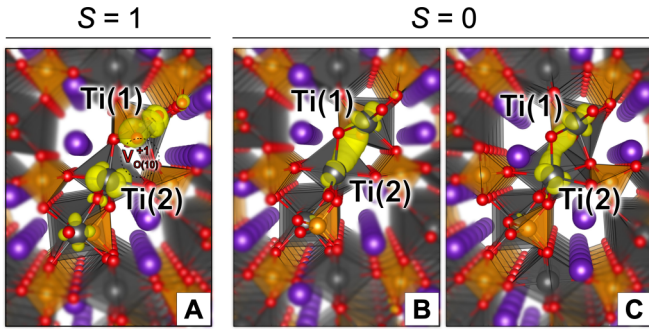


FIG. 5. Charge density related to the occupied midgap defect levels of the vacancy $V_{O(10)}^0$ calculated in the triplet ($S = 1$) ground state (configuration A) and two nonequivalent singlet ($S = 0$) spin configurations (configurations B and C).

method to be up to 0.5 eV, which correspond to the maximum difference in the peak positions with respect to the $GW + BSE$ spectra. The limited resolution of the present $GW + BSE$ calculations due to the restricted Brillouin zone sampling clearly hampers the comparison. For example, the defect signature in the zz component of the dielectric function appears only as a weak shoulder in the $GW + BSE$. Still, the data obtained here for the $V_{O(1)}$ vacancy suggest that PBE0-10% is a viable method to characterize the optical absorption due to both bulk and defect states in KTP.

B. Vacancy $V_{O(10)}$

The vacancy $V_{O(10)}$ can assume three different charge states ($q = +2, +1$, and 0). The ground state of the neutral vacancy is a spin triplet ($S = 1$), where two singly occupied Ti $3d$ -related one-particle states occur in the gap, localized at Ti(1) and Ti(2) near the vacancy (see configuration A in Fig. 5). Two spin-singlet ($S = 0$) configurations, with both electrons localized in a single orbital, are calculated to be 1.03 and 1.24 eV higher in energy (see configurations B and C, respectively, in Fig. 5). Although these diamagnetic, i.e., EPR-silent, configurations are energetically less favorable, they may form

upon charge transition or optical excitation and thus be visible in the optical response.

In Fig. 6 the diagonal components of the calculated dielectric function of KTP hosting an oxygen vacancy $V_{O(10)}^q$ in its three possible charge states are shown together with the KTP bulk optical response. The calculations are performed within the IPA using the PBE0-10% electronic structure. Obviously, the vacancy formation leads to a redistribution of the oscillator strength for the first main absorption peak (around 4.5 eV) to energies within the optical gap, especially for ε_{zz} and $q = 0, +1$. The charge state $q = +2$ does not feature any midgap defect level or related absorption. All Ti^{3+} -related defect levels remain empty and yield resonances in the conduction bands. Due to the defect-related relaxation of the selection rules, electronic transitions from the upper valence band into these states contribute to the absorption. They manifest themselves mainly in the shoulder, which arises on the low-energy side of the main absorption peak, in the energy range between 3 and 4 eV. Its intensity is highest in the charge state $+2$ but remains still visible (in decreasing order) in $q = +1$ and $q = 0$, where one and two levels are populated by the extra electrons, respectively.

The occupied gap levels in the charge states $+1$ and 0 give rise to a broad absorption band in the optical gap, which covers the whole near-infrared and visible spectrum. Thereby, the optical absorption is strongly polarization dependent: It is highest for the zz component and decreases successively for yy and xx . In z polarization, three relative maxima ($a_{1,2,3}$) can be identified in the energy range 0.5–2.5 eV for the EPR-active $V_{O(10)}^{+1}$ configuration, featuring one occupied defect level. They can be attributed to electronic transitions from the occupied gap level to the unoccupied Ti^{3+} levels located in the lower part of the conduction band ($a_{1,2}$) and into Ti $3d$ resonances (a_3) in the lower part of the conduction band, respectively. Notably, the neutral charge state within the $S = 1$ spin configuration leads to an absorption similar to that of the charge state $+1$. Both $S = 0$ defect geometries, however, give rise to a much enhanced optical absorption in the band gap, also regarding the xx and yy components. In fact, both

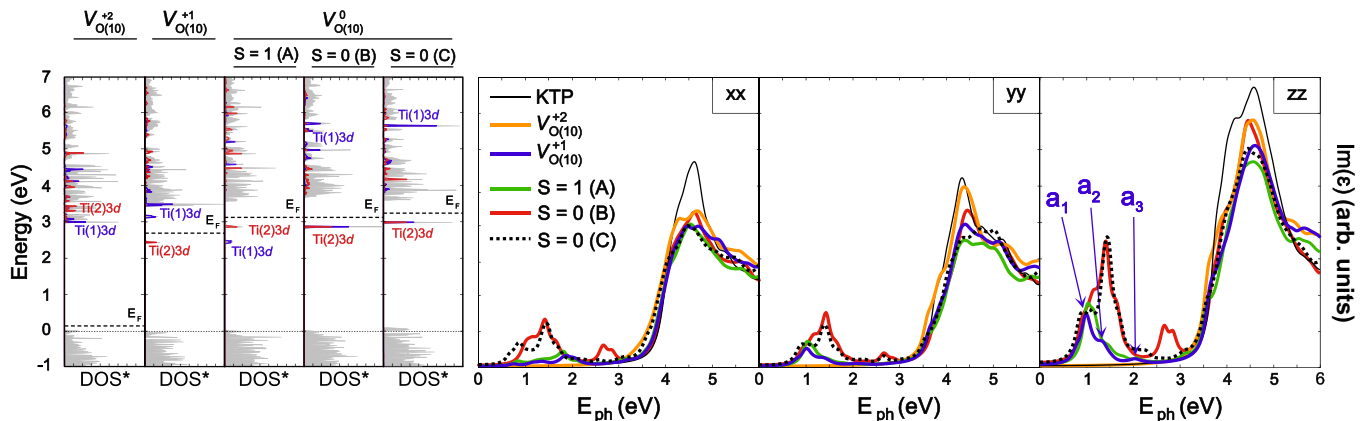


FIG. 6. Calculated diagonal components of the imaginary part of the dielectric function ε for KTP containing a vacancy $V_{O(10)}$ in the three possible charge states ($+2, +1$, and 0) in comparison to ideal bulk (thin solid black line; right panels) and their renormalized density of states (DOS*; left panels). Here, “A” corresponds to the $S = 1$ spin configuration, and “B” and “C” correspond to the two $S = 0$ spin configurations, shown in Fig. 5. The $+2$ charge state does not feature any gap state. One and two Ti $3d$ levels are occupied for $q = +1$ and $q = 0$, respectively. E_{ph} , photon energy.

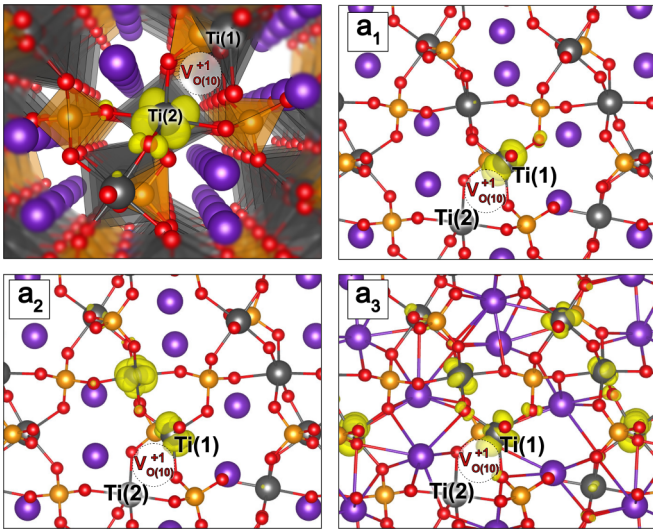


FIG. 7. Contribution of the wave function to the charge density of the occupied midgap defect level of the vacancy $V_{\text{O}(10)}^{+1}$ (top left) as well as those of the unoccupied defect levels and conduction bands corresponding to the $a_{1,2,3}$ absorption peaks.

configuration B and configuration C show not only a broader and higher absorption band in the energy range 0.5–2.0 eV, but also an additional absorption band in the ranges 2.4–3.2 eV (configuration B) and 2.0–2.3 eV (configuration C), respectively. These can be attributed to transitions from the occupied defect level into the Ti(1) 3*d* states located at about 5.6 eV (configuration B) and 5.0 eV (configuration C).

The charge transfer in Ti^{3+} - Ti^{4+} pairs has been discussed [10,57] as being responsible for an increase in optical absorption related to the gray-track formation. This finding is supported by the present results, as can be seen in Fig. 7, where the initial state as well as three final states corresponding to the $a_{1,2,3}$ peaks are shown. It can be seen that the optical transitions correspond largely to a charge transfer from Ti(2) to Ti(1)-related states.

The computational finding that the O-vacancy absorption is highest for *z*-polarized light, irrespective of the charge state, agrees with the observation that the crystals' resistance to gray tracking is weakest for laser beams polarized parallel to the *z* axis [7,8]. The dependence of the mid-gap absorption on the vacancy's charge state also suggests that the gray-track formation is related to O vacancies: It was found that the resistance against gray tracking is enhanced for Pb-doped material [58,59], while crystals with a higher K-vacancy concentration are particularly strongly affected by gray-track formation [13,18]. The replacement of K^+ with Pb^{2+} will lower the Fermi energy and thus increase the probability for twofold positively charged O vacancies with little absorption in the band gap, while low K concentrations are expected to increase the Fermi energy and thus the concentration of the more strongly absorbent $V_{\text{O}(10)}^{+1}$ and $V_{\text{O}(10)}^0$ [24] (cf. Fig. 6).

It was observed that the absorption of 1064-nm (1.17-eV) light increases in the initial state of gray tracking [60,61]. In addition, experiments showed that gray tracks give rise to a wide absorption band, covering the whole visible spectrum and the near-ultraviolet spectrum with maxima for the range between 380 and 440 nm and the range between 500

and 600 nm [9], respectively (2.82–3.26 and 2.07–2.48 eV, respectively). As discussed in Sec. III A, the accuracy of the PBE0-10% optical spectra is limited. In addition, the present calculations do not account for thermal broadening and the motional relaxation of selection rules. Still, they are in accord with the experimental findings. Notably, the strongest absorption of $V_{\text{O}(10)}^{+1}$ is located in the range between 0.8 and 1.3 eV corresponding to the initial stage of gray tracking. The metastable spin-singlet ($S = 0$) configurations of the neutral charge state, on the other hand, match the high-energy absorption maxima (around 2.3 and 3.0 eV) discussed in Ref. [9].

Thus our calculations corroborate the picture that defect-stabilized electron-hole pairs formed upon optical excitation transform $V_{\text{O}(10)}^{+2}$ into $V_{\text{O}(10)}^{+1}$ and $V_{\text{O}(10)}^0$ and thus increase the optical absorption by promoting the formation of gray tracks. In addition, the excitation of defect states may explain the broad luminescence in the energy range of 1–1.8 eV that was observed subsequent to irradiation with a 514.5-nm (2.4-eV) argon laser [62].

IV. CONCLUSION

The signatures of O vacancies in the KTP optical absorption were explored using hybrid DFT. A modified PBE0 functional containing 10% exact exchange was found to allow for the modeling of localized defect states and to provide optical excitation energies in fair agreement with *GW* + BSE data.

The calculations suggest oxygen vacancies at the O(10) site to be responsible for gray tracking, i.e., photochromic damage of the material. More precisely, the computational findings suggest that O vacancies are related to gray tracking not only due to their charge-compensating properties, but also due to their optical absorption: The calculated spectra for the $q = +1$ and neutral charge state in the $S = 1$ spin configuration are dominated by defect-related peaks at 1.1 eV, in agreement with the experimental observation that in the initial stage of gray tracking the absorption of 1064-nm (1.17-eV) light increases. In addition, the neutral $S = 0$ spin configurations give rise to an optical absorption that matches the measured absorption maxima characteristic for gray tracks [9]. The calculated midgap optical absorption depends strongly on the light polarization. It is highest for *z*-polarized light, in agreement with the experimental observation that the crystals' resistance to gray tracking is weakest for laser beams polarized parallel to the *z* axis [7,8]. The present calculations find the O-vacancy absorption to depend on the charge state. It is weakest for the +2 charge state and successively increases for the +1 and the neutral charge. This suggests Fermi level lowering as a means to suppress the optical absorption leading to gray tracking.

While the present computational results clearly indicate that O-vacancy-related light absorption is instrumental for the initial stages of gray tracking, the subsequent steps that include structural modifications still need to be understood.

ACKNOWLEDGMENT

Financial support from the Deutsche Forschungsgemeinschaft (DFG) via Grant No. TRR142/3-2022 (Project No.

231447078) and computational resources provided by the Paderborn Center for Parallel Computing (PC²) and the High

Performance Computing Center Stuttgart (HLRS) are gratefully acknowledged.

- [1] J. D. Bierlein and H. Vanherzeele, *J. Opt. Soc. Am. B* **6**, 622 (1989).
- [2] F. C. Zumsteg, J. D. Bierlein, and T. E. Gier, *J. Appl. Phys. (Melville, NY)* **47**, 4980 (1976).
- [3] B. Boulanger, M. M. Fejer, R. Blachman, and P. F. Bordui, *Appl. Phys. Lett.* **65**, 2401 (1994).
- [4] A. H. Reshak, I. V. Kityk, and S. Auluck, *J. Phys. Chem. B* **114**, 16705 (2010).
- [5] K. Kato, *IEEE J. Quantum Electron.* **28**, 1974 (1992).
- [6] M. G. Roelofs, *J. Appl. Phys. (Melville, NY)* **65**, 4976 (1989).
- [7] B. Boulanger, I. Rousseau, J. P. Feve, M. Maglione, B. Menaert, and G. Marnier, *IEEE J. Quantum Electron.* **35**, 281 (1999).
- [8] V. A. Maslov, V. A. Mikhailov, O. P. Shaunin, and I. A. Shcherbakov, *Quantum Electron.* **27**, 356 (1997).
- [9] N. B. Angert, V. M. Garmash, N. I. Pavlova, and A. V. Tarasov, *Sov. J. Quantum Electron.* **21**, 426 (1991).
- [10] G. M. Loiacono, D. N. Loiacono, T. McGee, and M. Babb, *J. Appl. Phys. (Melville, NY)* **72**, 2705 (1992).
- [11] Q. Zhang, G. Feng, J. Han, B. Li, Q. Zhu, and X. Xie, *Optik* **122**, 1313 (2011).
- [12] L. E. Halliburton and M. P. Sripsick, *Proc. SPIE* **2379**, 235 (1995).
- [13] M. Roth, in *Springer Handbook of Crystal Growth*, edited by G. Dhanaraj, K. Byrappa, V. Prasad, and M. Dudley (Springer, Berlin, 2010), Chap. 20, pp. 691–723.
- [14] N. I. Sorokina and V. I. Voronkova, *Crystallogr. Rep.* **52**, 80 (2007).
- [15] K. Momma and F. Izumi, *J. Appl. Crystallogr.* **44**, 1272 (2011).
- [16] J. E. Lowther, P. Manyum, and P. Suebka, *Phys. Status Solidi B* **242**, 1392 (2005).
- [17] D. Xue and S. Zhang, *Appl. Phys. Lett.* **70**, 943 (1997).
- [18] Y. Zhang, J. Li, X. Cao, J. Yang, J. Wang, and H. Jiang, *AIP Adv.* **4**, 127103 (2014).
- [19] A. Bocchini, S. Neufeld, U. Gerstmann, and W. G. Schmidt, *J. Phys.: Condens. Matter* **31**, 385401 (2019).
- [20] M. P. Sripsick, G. J. Edwards, L. E. Halliburton, R. F. Belt, and G. M. Loiacono, *J. Appl. Phys. (Melville, NY)* **76**, 773 (1994).
- [21] S. D. Setzler, K. T. Stevens, N. C. Fernelius, M. P. Sripsick, G. J. Edwards, and L. E. Halliburton, *J. Phys.: Condens. Matter* **15**, 3969 (2003).
- [22] G. J. Edwards, M. P. Sripsick, L. E. Halliburton, and R. F. Belt, *Phys. Rev. B* **48**, 6884 (1993).
- [23] Y. Zhang, Y. Leng, J. Liu, N. Ji, X. Duan, J. Li, X. Zhao, J. Wang, and H. Jiang, *CryEngComm* **17**, 3793 (2015).
- [24] A. Bocchini, C. Eigner, C. Silberhorn, W. G. Schmidt, and U. Gerstmann, *Phys. Rev. Materials* **4**, 124402 (2020).
- [25] S. Neufeld, A. Bocchini, U. Gerstmann, A. Schindlmayr, and W. G. Schmidt, *J. Phys. Mater.* **2**, 045003 (2019).
- [26] P. Giannozzi, S. Baroni, N. Bonini, M. Calandra, R. Car, C. Cavazzoni, D. Ceresoli, G. L. Chiarotti, M. Cococcioni, I. Dabo, A. D. Corso, S. de Gironcoli, S. Fabris, G. Fratesi, R. Gebauer, U. Gerstmann, C. Gougoussis, A. Kokalj, M. Lazzeri, L. Martin-Samos *et al.*, *J. Phys.: Condens. Matter* **21**, 395502 (2009).
- [27] P. Giannozzi, O. Andreussi, T. Brumme, O. Bunau, M. B. Nardelli, M. Calandra, R. Car, C. Cavazzoni, D. Ceresoli, M. Cococcioni, N. Colonna, I. Carnimeo, A. D. Corso, S. de Gironcoli, P. Delugas, R. A. DiStasio, A. Ferretti, A. Floris, G. Fratesi, G. Fugallo *et al.*, *J. Phys.: Condens. Matter* **29**, 465901 (2017).
- [28] J. P. Perdew, A. Ruzsinszky, G. I. Csonka, O. A. Vydrov, G. E. Scuseria, L. A. Constantin, X. Zhou, and K. Burke, *Phys. Rev. Lett.* **100**, 136406 (2008); **102**, 039902(E) (2009).
- [29] M. Cococcioni and S. de Gironcoli, *Phys. Rev. B* **71**, 035105 (2005).
- [30] C. Ricca, I. Timrov, M. Cococcioni, N. Marzari, and U. Aschauer, *Phys. Rev. Research* **2**, 023313 (2020).
- [31] I. Timrov, N. Marzari, and M. Cococcioni, *Phys. Rev. B* **98**, 085127 (2018).
- [32] D. Sangalli, A. Ferretti, H. Miranda, C. Attaccalite, I. Marri, E. Cannuccia, P. Melo, M. Marsili, F. Paleari, A. Marrazzo, G. Prandini, P. Bonfà, M. O. Atambo, F. Affinito, M. Palummo, A. Molina-Sánchez, C. Hogan, M. Grüning, and D. Varsano, *J. Phys.: Condens. Matter* **31**, 325902 (2019).
- [33] A. Marini, C. Hogan, M. Grüning, and D. Varsano, *Comput. Phys. Commun.* **180**, 1392 (2009).
- [34] W. G. Schmidt, *Phys. Status Solidi B* **242**, 2751 (2005).
- [35] L. Hedin, *Phys. Rev.* **139**, A796 (1965).
- [36] F. Bechstedt, *Many-Body Approach to Electronic Excitations: Concepts and Applications*, 1st ed. (Springer-Verlag, Berlin, 2015).
- [37] M. Rohlfing and S. G. Louie, *Phys. Rev. Lett.* **81**, 2312 (1998).
- [38] G. Onida, L. Reining, and A. Rubio, *Rev. Mod. Phys.* **74**, 601 (2002).
- [39] W. G. Schmidt, S. Glutsch, P. H. Hahn, and F. Bechstedt, *Phys. Rev. B* **67**, 085307 (2003).
- [40] H. Li, C. Kam, Y. Lam, and W. Ji, *Opt. Mater. (Amsterdam)* **15**, 237 (2001).
- [41] M. Sheik-Bahae, D. Hutchings, D. Hagan, and E. Van Stryland, *IEEE J. Quantum Electron.* **27**, 1296 (1991).
- [42] A. Dudelzak, P.-P. Proulx, V. Denks, V. Mürk, and V. Nagirnyi, *J. Appl. Phys. (Melville, NY)* **87**, 2110 (2000).
- [43] J. Jaramillo, G. E. Scuseria, and M. Ernzerhof, *J. Chem. Phys.* **118**, 1068 (2003).
- [44] J. Muscat, A. Wander, and N. Harrison, *Chem. Phys. Lett.* **342**, 397 (2001).
- [45] M. Marsman, J. Paier, A. Stroppa, and G. Kresse, *J. Phys.: Condens. Matter* **20**, 064201 (2008).
- [46] C. Franchini, V. Bayer, R. Podloucky, J. Paier, and G. Kresse, *Phys. Rev. B* **72**, 045132 (2005).
- [47] M. Betzinger, C. Friedrich, and S. Blügel, *Phys. Rev. B* **81**, 195117 (2010).
- [48] A. M. Navarete-López, M. Rivera-Almazo, J. Garza, and R. Vargas, *Theor. Chem. Acc.* **137**, 36 (2018).
- [49] H.-P. Komsa, P. Broqvist, and A. Pasquarello, *Phys. Rev. B* **81**, 205118 (2010).

- [50] A. Janotti, J. B. Varley, P. Rinke, N. Umezawa, G. Kresse, and C. G. Van de Walle, *Phys. Rev. B* **81**, 085212 (2010).
- [51] P. Deák, M. Lorke, B. Aradi, and T. Frauenheim, *J. Appl. Phys. (Melville, NY)* **126**, 130901 (2019).
- [52] J. P. Perdew, M. Ernzerhof, and K. Burke, *J. Chem. Phys.* **105**, 9982 (1996).
- [53] J. P. Perdew, K. Burke, and M. Ernzerhof, *Phys. Rev. Lett.* **77**, 3865 (1996).
- [54] S. Albrecht, L. Reining, R. Del Sole, and G. Onida, *Phys. Rev. Lett.* **80**, 4510 (1998).
- [55] L. X. Benedict, E. L. Shirley, and R. B. Bohn, *Phys. Rev. Lett.* **80**, 4514 (1998).
- [56] M. Ghoohestani, S. J. Hashemifar, and A. Arab, *J. Appl. Phys. (Melville, NY)* **128**, 125707 (2020).
- [57] M. N. Satyanarayan, A. Deepthy, and H. L. Bhat, *Crit. Rev. Solid State Mater. Sci.* **24**, 103 (1999).
- [58] K. T. Stevens, L. E. Halliburton, M. Roth, N. Angert, and M. Tseitlin, *J. Appl. Phys. (Melville, NY)* **88**, 6239 (2000).
- [59] Y. Zhang, H. Wang, C. Ma, Y. Jia, J. Li, J. Wang, R. Boughton, and H. Jiang, *J. Cryst. Growth* **412**, 67 (2015).
- [60] A. Alexandrovski, M. Fejer, and G. Mitchell, in *Technical Digest. Summaries of Papers Presented at the Conference on Lasers and Electro-Optics. Postconference Edition. CLEO '99. Conference on Lasers and Electro-Optics (IEEE, Piscataway, NJ, 1999)*, pp. 531–532.
- [61] M. Roth, N. Angert, M. Tseitlin, and A. Alexandrovski, *Opt. Mater. (Amsterdam)* **16**, 131 (2001).
- [62] A. Deepthy, K. S. R. K. Rao, H. L. Bhat, R. Kumar, and K. Asokan, *J. Appl. Phys. (Melville, NY)* **89**, 6560 (2001).